Magnetization relaxation dynamics in polydisperse ferrofluids

Alexey O. Ivanov ®

Department of Theoretical and Mathematical Physics, Ural Mathematical Center, Institute of Natural Sciences and Mathematics,
Ural Federal University, 51 Lenin Avenue, Ekaterinburg 620000, Russia

Philip J. Camp ®*

School of Chemistry, University of Edinburgh, David Brewster Road, Edinburgh EH9 3FJ, Scotland

When a ferrofluid is magnetized in a strong magnetic field, and then the field is switched off, the magnetization decays from its saturation value to zero. The dynamics of this process are controlled by the rotations of the constituent magnetic nanoparticles, and for the Brownian mechanism, the respective rotation times are strongly influenced by the particle size and the magnetic dipole-dipole interactions between the particles. In this work, the effects of polydispersity and interactions on the magnetic relaxation are studied using a combination of analytical theory and Brownian dynamics simulations. The theory is based on the Fokker-Planck-Brown equation for Brownian rotation and includes a self-consistent, mean-field treatment of the dipole-dipole interactions. The most interesting predictions from the theory are that, at short times, the relaxation of each particle type is equal to its intrinsic Brownian rotation time, while at long times, each particle type has the same effective relaxation time, which is longer than any of the individual Brownian rotation times. Noninteracting particles, though, always relax at a rate controlled only by the Brownian rotation times. This illustrates the importance of including the effects of polydispersity and interactions when analyzing the results from magnetic relaxometry experiments on real ferrofluids, which are rarely monodisperse.

I. INTRODUCTION

Ferrofluids are colloidal suspensions of magnetic nanoparticles in a nonmagnetic carrier liquid [1]. Much of the interest and utility of ferrofluids lies in the response to static and ac magnetic fields. The magnetization curve, initial static susceptibility, and dynamic magnetic susceptibility are all important properties for technological applications of ferrofluids. The dynamics of the magnetic nanoparticles are particularly important. Each particle carries a magnetic dipole moment, and this can reorient through two main mechanisms: Brownian rotation of the particle as a whole, at a rate controlled by the particle volume, liquid viscosity, and temperature; and Néel rotation of the dipole moment within the particle, at a rate controlled by the particle volume, magnetic anisotropy energy, and temperature. For small particles, Néel rotation is dominant, while for large particles, Brownian rotation is dominant [2]. The reorientational dynamics are clearly dependent on particle size—and hence the polydispersity of the ferrofluid—but also on magnetic dipole-dipole interactions between the particles. The effective rotation times dictate the response of the magnetization to ac magnetic fields and the dissipation of energy as heat, which can be applied in biomedical contexts [3,4]. The dynamical response could also be used for

magnetic granulometric characterization of ferrofluids. Existing methods for determining the particle-size distribution include various forms of microscopy, and fitting the magnetization curve using accurate theoretical expressions [5–7]. But the dynamical response can also be analyzed, and a fitted distribution of relaxation times can be connected with the particle-size distribution [8,9]. Moreover, the dynamic magnetic susceptibility can also be used to characterize anisotropic particles, such as magnetic platelets [10]. Another important dynamical property of ferrofluids is the relaxation of the magnetization from an initial, strongly aligned state [11–19]. In this case, the ferrofluid is magnetized in a static magnetic field, the field is switched off, and the magnetization is measured as a function of time. The resulting magnetic relaxation curve contains contributions with different decay rates, depending on the particle-size distribution, and the interactions between particles.

A recent theoretical study [20] was dedicated to the effects of polydispersity and interactions on related but different dynamical properties: the dynamic magnetic susceptibility, and the underlying *equilibrium* magnetization autocorrelation function in zero field; and the magnetic relaxation curve, and its frequency spectrum. Note that these two groups of properties are similar, but not equivalent, because the dynamic magnetic susceptibility characterizes the response to weak ac fields, and is related to the autocorrelation function by linear-response theory, while the magnetic relaxation curve describes the decay starting from the strong-field regime. Nonetheless, the effects of interactions on the relaxation times in monodisperse ferrofluids are well understood, and comparable in the two cases [21,22]. The effects of polydispersity

---

*philip.camp@ed.ac.uk

on the dynamic magnetic susceptibility have also been thoroughly studied [23]. In Ref. [20], the effects of polydispersity on the magnetic relaxation curve were analyzed using a theory based on the Fokker-Planck-Brown (FPB) equation describing Brownian rotational diffusion [24–26], and including the magnetic dipole-dipole interactions between particles. It was found that the instantaneous and effective relaxation times evolved during the process in a complex way. At the start of the magnetization decay, the effective relaxation times coincide with the Brownian rotation times for noninteracting particles. At long times, the effective relaxation time for each particle type converges onto one value, which is longer than any one of the Brownian rotation times. A simple explanation is that, at long times, the local magnetic field experienced by a particle is dominated by the fields produced by the larger particles, and the larger particles are the ones that relax slowest. Hence, all of the particles are slaved to the remaining magnetization of the large particles, leading to one characteristic relaxation time. This time is longer than any of the Brownian rotation times due to the effects of interactions. If interactions are ignored, no such effect is predicted, and each type of particle relaxes with its own Brownian time.

The aim of this work is to test the theoretical predictions for the magnetic relaxation curves in polydisperse ferrofluids using Brownian dynamics (BD) simulations. To this end, the work on monodisperse ferrofluids in Ref. [22] is extended to model bidisperse and tridisperse ferrofluids. The FPB theory, with interactions, is adapted to handle distinct particle types, with different dipole moments and Brownian rotation times. BD simulations are carried out on several different model ferrofluids, and the computed magnetic relaxation curves are compared with the theoretical predictions. It is shown that the simulation results are consistent with the theory, and confirm that the effects of polydispersity and interactions on the magnetic relaxation are significant. The merit of studying polydisperse systems with only two or three fractions, with distinct Brownian rotation times, is that it is possible to distinguish clearly between the dynamics of small, medium, and large particles, and the extent to which small particles are affected by the larger ones. The particle-size distributions in real ferrofluids are more continuous, with log-normal or gamma probability distribution functions often being used in modeling, but then the distinction between small and large particles becomes blurred, and this makes it difficult to test some of the predictions of the theory. Note that bidisperse models already capture a lot of polydispersity-related effects in real ferrofluids [27–29].

The rest of this article is organized as follows. The model, theory, simulation methods, and chosen systems are detailed in Sec. II. The results are presented in Sec. III, addressing first the basic appearance of the magnetic relaxation curves in each of the systems being studied, and then the evolution of the effective relaxation times throughout the decay process. Section IV concludes the article.

II. MODEL AND METHODS

A. Model

The ferrofluid is modeled as a system of N homogeneously magnetized spherical particles in a volume V at temperature

T. The total particle number concentration is $\rho = N/V$. The particles are polydisperse, and the number fraction of particles with diameter σ_k, and magnetic moment μ_k, is p_k, with $\sum_k p_k = 1$. It is assumed that the magnetic anisotropy energy of the particles greatly exceeds the thermal energy $k_B T$, and so the magnetic moment is "frozen" inside the particle body. This means that the particle magnetic moment can reorient only by the Brownian mechanism of particle rotation, and the characteristic Brownian rotation time of fraction k is τ_k. For a given magnetic material with saturation magnetization M_{sat}, the magnetic dipole moment is $\mu_k = \pi M_{\text{sat}} \sigma_k^3 / 6$. For a carrier liquid with viscosity η, the Brownian rotation time is $\tau_k = \pi \eta \sigma_k^3 / 2 k_B T$. Although suitable dimensionless units will be used throughout this work, these dependencies of μ_k and τ_k on σ_k will be satisfied.

The ferrofluid is assumed to be in a highly elongated cylindrical container aligned along the laboratory z axis, and the external magnetic field $\boldsymbol{H} = (0, 0, H)$ is applied in the same direction. The shape of the container means that demagnetization effects can be neglected, and the internal magnetic field can be taken to be the same as the external applied field $\boldsymbol{H}$. Particle i interacts with the external magnetic field with the Zeeman energy $u_Z(i)$, and with another particle j through the combination of a short-range, isotropic repulsive interaction $u_s(i, j)$ preventing particle overlaps (specified later), and the magnetic dipole-dipole interaction $u_d(i, j)$:

$$u_Z(i) = -\mu_0 (\boldsymbol{\mu}_i \cdot \boldsymbol{H}), \tag{1}$$

$$u_d(i, j) = \frac{\mu_0}{4\pi} \left[\frac{(\boldsymbol{\mu}_i \cdot \boldsymbol{\mu}_j)}{r_{ij}^3} - \frac{3(\boldsymbol{\mu}_i \cdot \boldsymbol{r}_{ij})(\boldsymbol{\mu}_j \cdot \boldsymbol{r}_{ij})}{r_{ij}^5} \right]. \tag{2}$$

Here μ_0 is the vacuum magnetic permeability, and $\boldsymbol{r}_{ij}$ is the center-to-center separation vector between particles i and j. The dipole-dipole interaction (2) is correct for homogeneously magnetized spheres [30]. The collective behavior of the ferrofluid is controlled by the particle volume fraction φ, the dipolar coupling constant λ, and the Langevin susceptibility χ, defined as follows:

$$\varphi = \frac{\pi \rho}{6} \sum_k p_k \sigma_k^3 = \frac{\pi \rho \langle \sigma^3 \rangle}{6}, \tag{3}$$

$$\lambda = \frac{\mu_0}{4\pi k_B T} \frac{\sum_k p_k \mu_k^2}{\sum_k p_k \sigma_k^3} = \frac{\mu_0}{4\pi k_B T} \frac{\langle \mu^2 \rangle}{\langle \sigma^3 \rangle}, \tag{4}$$

$$\chi = \frac{\mu_0 \rho}{3 k_B T} \sum_k p_k \mu_k^2 = 8 \lambda \varphi. \tag{5}$$

The angled brackets $\langle \cdots \rangle = \sum_k \cdots p_k$ denote an average over the particle size distribution. Note that the Langevin susceptibility is usually distinguished from the actual susceptibility by a subscript "L," but it is omitted here to simplify the notation.

B. Theory

The orientation of each particle magnetic moment with respect to the external magnetic field is characterized by the angle $\theta = \angle(\boldsymbol{\mu}, \boldsymbol{H})$, and the corresponding time-dependent, one-particle probability density is denoted by $W(\theta, t)$. This probability is determined by three factors: thermal

fluctuations, dipole-field coupling, and interparticle interactions. In the classical approach for noninteracting particles, and for a randomly chosen particle i, the density $W_0(\theta_i, t) \equiv W_0(i)$ is the solution of the FPB equation [24–26],

$$2\tau_i \frac{\partial W_0(i)}{\partial t} = \frac{\partial}{\partial z_i}\left\{(1-z_i^2)\left[\frac{\partial W_0(i)}{\partial z_i} + \frac{W_0(i)}{k_BT}\frac{\partial u_Z(i)}{\partial z_i}\right]\right\}, \quad (6)$$

where $z_i = \cos\theta_i$. The problem is that this equation holds true only for noninteracting particles. To account for the interparticle interactions, the following extension of the FPB equation was proposed in Refs. [31] and [22]. The main idea is that each particle i interacts with the external magnetic field $\boldsymbol{H}$ plus the magnetic field $\boldsymbol{H}_d$ produced by all other dipoles in the system, giving a total, effective field

$$\boldsymbol{H}_{\mathrm{eff}} = \boldsymbol{H} + \boldsymbol{H}_d. \quad (7)$$

So the energy $u_Z(i)$ in Eq. (6) is to be replaced by the effective, one-particle energy

$$u_{\mathrm{eff}}(i) = -\mu_0(\boldsymbol{\mu}_i \cdot \boldsymbol{H}_{\mathrm{eff}}), \quad (8)$$

giving the modified FPB equation

$$2\tau_i \frac{\partial W(i)}{\partial t} = \frac{\partial}{\partial z_i}\left\{(1-z_i^2)\left[\frac{\partial W(i)}{\partial z_i} + \frac{W(i)}{k_BT}\frac{\partial u_{\mathrm{eff}}(i)}{\partial z_i}\right]\right\}. \quad (9)$$

Evidently, $\boldsymbol{H}_d$ takes into account the interparticle dipolar correlations between any two particles. To calculate it, one needs to take the magnetic field produced by a randomly chosen particle j at the position of particle i, and integrate over all possible positions, orientations, and sizes of particle j inside the sample container, weighted by the particle-size distribution, and the one-particle probability density $W(j)$:

$$\boldsymbol{H}_d = \frac{\rho}{4\pi}\left\langle\!\left\langle\left[\frac{3\boldsymbol{r}_{ij}(\boldsymbol{\mu}_j \cdot \boldsymbol{r}_{ij})}{r_{ij}^5} - \frac{\boldsymbol{\mu}_j}{r_{ij}^3}\right]W(j)\right\rangle\!\right\rangle_j. \quad (10)$$

The double angled brackets $\langle\!\langle\dots\rangle\!\rangle_j$ denote the aforementioned averaging for particle j. To evaluate $\boldsymbol{H}_d$ requires $W(j)$, which is of course the desired solution of the modified FPB equation. Using an approach similar to Weiss mean-field theory [32], a self-consistent solution can obtained by linking Eqs. (9) and (10) together through the overall magnetization in the field direction, equal to

$$M = \rho \sum_k p_k \mu_k m_k, \quad (11)$$

where the fractional magnetization of a particle of type k is

$$m_k = \frac{1}{2}\int_{-1}^{1} z_k W_k \, dz_k. \quad (12)$$

Note that W_k means the one-particle probability density for particles of *type* k, rather than for a particular particle. Performing the positional integration in Eq. (10), and taking into account the indistinguishability of particles in each fraction, the effective dipole field appears to be uniform, aligned along the field direction, and equal to

$$\boldsymbol{H}_d = \left(\frac{M}{3}\right)\frac{\boldsymbol{H}}{H}. \quad (13)$$

Now the development is focused on the particular situation of interest, in which the system is magnetized in an external magnetic field, and then the field is switched off. The magnetization $M(t)$ decreases with time, and the resulting FPB Eq. (9) for the probability density for particles of type k, rather than for a particular particle, is

$$2\tau_k \frac{\partial W_k}{\partial t} = \frac{\partial}{\partial z_k}\left\{(1-z_k^2)\left[\frac{\partial W_k}{\partial z_k} - \frac{\mu_0\mu_k W_k M(t)}{3k_BT}\right]\right\}. \quad (14)$$

This equation is solved by expanding $W_k = W_k(\cos\theta, t)$ as a sum of Legendre polynomials, according to the method presented in Ref. [22]. This results in the following equation for the first moment m_k of the probability density:

$$\frac{dm_k(t)}{dt} = -\frac{1}{\tau_k}\left\{m_k(t) - \frac{\mu_0\mu_k M(t)}{9k_BT}[1 - e^{-3t/\tau_k}]\right\}. \quad (15)$$

There is a set of equations for the fractional magnetizations m_k of all particle types, and all equations are coupled by the overall magnetization M in Eq. (11). In what follows, these equations are solved numerically for several ferrofluid samples with a small number of particle types, as defined in Sec. II D. This was carried out with Mathcad [33] using the fourth-order Runge-Kutta fixed-step method (Mathcad `rkfixed` function). The relative tolerance for the convergence of numerical solutions was set to 10^{-5}.

Some important features of the magnetization relaxation process can be highlighted already. At short times, such that $t \ll \tau_k/3$ and the term in square brackets is very small, each fractional magnetization obeys the simple exponential decay

$$m_k(t) \approx e^{-t/\tau_k}, \quad (16)$$

i.e., the initial relaxation rate is independent of the coupling to other particles. This is, of course, also the solution for noninteracting particles, for which the term proportional to $\mu_k M(t)$ on the right-hand side of Eq. (15) is omitted. With interactions, the decay at longer times should depend on interactions in a complicated way because of the $\mu_k M(t)$ term, and an effective relaxation time can be defined for each fraction by the relation

$$\tau_{\mathrm{eff},k} \equiv -\left[\frac{d\ln m_k(t)}{dt}\right]^{-1}. \quad (17)$$

In the case of a monodisperse ferrofluid, or one in which the interactions between different fractions are somehow turned off, the asymptotic, long-time limit of Eq. (15) gives

$$\frac{dm_k(t)}{dt} = -\frac{m_k(t)}{\tau_k}\left(1 - \frac{\mu_0\rho p_k \mu_k^2}{9k_BT}\right), \quad (18)$$

and hence the effective relaxation time is $\tau_{\mathrm{eff},k} = \tau_k/(1 - \chi_k/3)$, where χ_k is the Langevin susceptibility of fraction k [see Eq. (5)]. The apparent divergence in the relaxation time when $\chi_k = 3$ is a well-known artifact of the Weiss theory, signaling an apparent transition to a ferromagnetic liquid, but that will not cause problems here because the systems being studied have $\chi_k < 1$.

C. Simulations

BD simulations were carried out on mixtures of dipolar particles with short-range, repulsive interactions given by the Weeks-Chandler-Anderson (WCA) potential, equivalent to a

TABLE I. List of configurations containing small, medium, and large particles: bidisperse configuration A, $\tau_2/\tau_1 = 10$ and equal $p_k\mu_k^2$; bidisperse configuration B, $\tau_2/\tau_1 = 10$ and equal $p_k\mu_k$; tridisperse configuration C, $\tau_3/\tau_2 = \tau_2/\tau_1 = \sqrt{10}$ and equal $p_k\mu_k$; bidisperse configuration D, $\tau_2/\tau_1 = 2$ and $p_1 = 0.9$; bidisperse configuration E, $\tau_2/\tau_1 = 2$ and $p_1 = 0.99$. In each case, $\langle\sigma^3\rangle = \tilde{\sigma}^3$, $\langle\mu^2\rangle = \tilde{\mu}^2$, $\langle\tau\rangle = \tilde{\tau}$, the volume fraction is $\varphi = 1/8$, the dipolar coupling constant is $\lambda = 1$, and the Langevin susceptibility is $\chi = 8\varphi\lambda = 1$. Also shown are the values of $p_k\mu_k/\langle\mu\rangle$ and $p_k\mu_k^2/\langle\mu^2\rangle = \chi_k$, the individual dipolar coupling constants $\lambda_k = \mu_0\mu_k^2/4\pi\sigma_k^3 k_B T$, and the numbers of particles of each type in the BD simulations of configurations A–D.

Configuration	Fraction k	p_k	$\sigma_k/\tilde{\sigma}$	$\mu_k/\tilde{\mu}$	$\tau_k/\tilde{\tau}$	$p_k\mu_k/\langle\mu\rangle$	$p_k\mu_k^2/\langle\mu^2\rangle$	λ_k	N_k
A	1 (small)	0.990099	0.971948	0.710634	0.918182	0.909091	0.500000	0.550000	3200
	2 (large)	0.009901	2.093998	7.106335	9.181818	0.090909	0.500000	5.500000	32
B	1 (small)	0.909091	0.819321	0.316228	0.550000	0.500000	0.090909	0.181818	3000
	2 (large)	0.090909	1.765174	3.162278	5.500000	0.500000	0.909091	1.818182	300
C	1 (small)	0.706101	0.778641	0.316228	0.472076	0.333333	0.070610	0.211830	2000
	2 (medium)	0.223289	1.142889	1.000000	1.492835	0.333333	0.223289	0.669866	632
	3 (large)	0.070610	1.677531	3.162278	4.720759	0.333333	0.706101	2.118303	200
D	1 (small)	0.900000	0.968729	0.877058	0.909091	0.818182	0.692308	0.846154	9000
	2 (large)	0.100000	1.220522	1.754116	1.818182	0.181818	0.307692	1.692308	1000
E	1 (small)	0.990000	0.996689	0.985329	0.990099	0.980198	0.961165	0.980583	–
	2 (large)	0.010000	1.255749	1.970659	1.980198	0.019802	0.038835	1.961165	–

cut-and-shifted Lennard-Jones (LJ) potential:

$$u_s(i,j) = \begin{cases} 4\varepsilon\left[\left(\frac{\sigma_{ij}}{r_{ij}}\right)^{12} - \left(\frac{\sigma_{ij}}{r_{ij}}\right)^6 + \frac{1}{4}\right] & r_{ij} \leqslant r_{ij}^{\text{cut}} \\ 0 & r_{ij} > r_{ij}^{\text{cut}} \end{cases}. \quad (19)$$

The LJ energy parameter $\varepsilon = k_B T$ is kept the same for all particle types, the LJ distance parameter $\sigma_{ij} = (\sigma_i + \sigma_j)/2$ is the arithmetic mean of the diameters of the two particles, and $r_{ij}^{\text{cut}} = 2^{1/6}\sigma_{ij}$ is the position of the minimum in the LJ potential. All relevant properties can be expressed in dimensionless form using basic units of mass m, length $\tilde{\sigma}$, energy ε, time $\tilde{t} = \sqrt{m\tilde{\sigma}^2/\varepsilon}$, and dipole moment $\tilde{\mu} = \sqrt{4\pi\tilde{\sigma}^3\varepsilon/\mu_0}$. Brownian dynamics (BD) simulations were carried out using LAMMPS [34–36]. As described elsewhere [21], LAMMPS is actually used to integrate the Langevin equations of motion with friction coefficients sufficiently large to damp inertial motion over a suitably short time scale, and rapidly enter the Brownian regime. This is easily determined by simulating noninteracting particles first, and checking that the magnetization decay starting from a fully aligned state is equal to Eq. (16). In practice, a good choice for the LAMMPS damping time (inversely proportional to the friction coefficient) is $t_{\text{damp}}^* = 1/20$ in LJ units, and this is scaled accordingly (using the `scale` arguments) to give the correct Brownian rotation times for solid spherical particles with different diameters, and equal mass density $\varrho = 6m/\pi\tilde{\sigma}^3$. The Brownian rotation time corresponding to this value of t_{damp}^*, and reduced temperature $T^* = k_B T/\varepsilon = 1$, is $\tilde{\tau}/\tilde{t} = 1/6T^* t_{\text{damp}}^* = 10/3$ [21]. The integration time step was $\delta t = 0.005\tilde{t}$.

For each configuration, the system was equilibrated in zero field, the particle dipole moments were instantaneously aligned, and then the subsequent decay of the magnetization (total and for each species) was computed. This was repeated 50 times for each configuration, and the mean values and standard errors were calculated. In earlier work on monodisperse systems [22], three protocols were tested, which differed in the way the system was equilibrated before initiating relaxation: in method A, the system was equilibrated in zero field,

with interactions, the dipole moments were instantaneously aligned, and then immediately allowed to relax; in method B, the system was equilibrated in zero field, but without interactions, and then the dipoles were aligned and relaxed; and in method C, the system was equilibrated with the dipoles perfectly aligned as if in an infinitely strong field, and then the field was switched off. In principle, these methods give different results because of the amount of structuring that can develop within the fluid prior to relaxation. Methods A and B give results that are closer to theory, because the theory does not capture chainlike correlations, although this would only be important when $\lambda \gg 1$. For the parameters chosen in this work, there is very little structuring, and as shown explicitly in Ref. [22], there is practically no difference between the protocols. The protocol used in this work is method A, and corresponds to a pulsed, aligning magnetic field.

D. Configurations

Five configurations were studied, as detailed in Table I. For each configuration, the number fraction p_k, diameter σ_k, dipole moment μ_k, and Brownian rotation time τ_k of fraction k are given. The averages $\langle\sigma^3\rangle = \tilde{\sigma}^3$, $\langle\mu^2\rangle = \tilde{\mu}^2$, and $\langle\tau\rangle = \tilde{\tau}$ are the same in each case. $\langle\tau\rangle$ will henceforth be taken as the natural unit of time. The volume fraction is $\varphi = 1/8$, the dipolar coupling constant is

$$\lambda = \frac{\mu_0}{4\pi k_B T}\frac{\langle\mu^2\rangle}{\langle\sigma^3\rangle} = \frac{\mu_0}{4\pi\varepsilon}\frac{\tilde{\mu}^2}{\tilde{\sigma}^3} = 1, \quad (20)$$

and the Langevin susceptibility is $\chi = 8\varphi\lambda = 1$. The five configurations A–E have the following characteristics.

Configuration A is bidisperse, and contains small ($k = 1$) and large ($k = 2$) particles: $\tau_2/\tau_1 = 10$, and each fraction has the same $p_k\mu_k^2$ and so contributes equally to the initial susceptibility.

Configuration B is bidisperse, and contains small ($k = 1$) and large ($k = 2$) particles: $\tau_2/\tau_1 = 10$, and each fraction
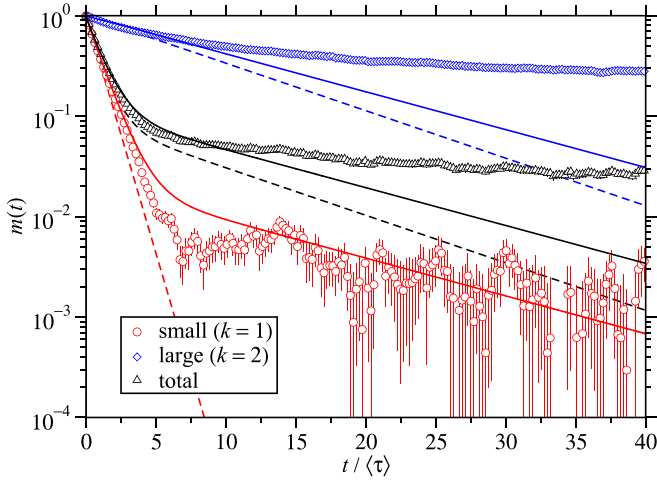
FIG. 1. Magnetic relaxation curves for bidisperse configuration A. The points are from BD simulations, the dashed lines are for noninteracting particles, and the solid lines are from the Weiss theory: red circles and lines, small particles ($k = 1$); blue diamonds and lines, large particles ($k = 2$); black triangles and lines, all particles.

FIG. 2. Magnetic relaxation curves for bidisperse configuration B. The points are from BD simulations, the dashed lines are for noninteracting particles, and the solid lines are from the Weiss theory: red circles and lines, small particles ($k = 1$); blue diamonds and lines, large particles ($k = 2$); black triangles and lines, all particles. The green dot-dashed lines are fits to the data in the range $t \geqslant 5\langle\tau\rangle$.

has equal $p_k\mu_k$ and so contributes equally to the saturation magnetization.

Configuration C is tridisperse, and contains small ($k = 1$), medium ($k = 2$), and large ($k = 3$) particles: $\tau_3/\tau_2 = \tau_2/\tau_1 = \sqrt{10}$, and each fraction has equal $p_k\mu_k$ and so contributes equally to the saturation magnetization.

Configuration D is bidisperse, and contains small ($k = 1$) and large ($k = 2$) particles: $\tau_2/\tau_1 = 2$ and $p_1 = 0.9$, chosen because of its interesting properties.

Configuration E is the same as configuration D, except that $p_1 = 0.99$.

Table I also shows the values of $p_k\mu_k$ and $p_k\mu_k^2$, the individual dipolar coupling constants $\lambda_k = \mu_0\mu_k^2/4\pi\sigma_k^3 k_B T$, and the number of particles of each type in the BD simulations. Note that because the overall Langevin susceptibility is $\chi = 1$, $p_k\mu_k^2/\langle\mu^2\rangle$ is also equal to the Langevin susceptibility χ_k of fraction k [see Eq. (5)]. Although only one value of the average dipolar coupling constant has been considered, the effects of stronger magnetic interactions have been included implicitly, because λ_k for the large particles is significantly larger than unity. The effects of large values of λ in monodisperse ferrofluids were reported in Ref. [22].

III. RESULTS

A. Bidisperse configuration A

Magnetic relaxation curves for bidisperse configuration A are shown in Fig. 1. The individual relaxation curves $m_k(t)$ are shown, along with the total relaxation curve

$$m(t) = \frac{1}{\langle\mu\rangle} \sum_k p_k\mu_k m_k(t). \tag{21}$$

Each fraction makes an equal contribution to the initial Langevin susceptibility, and as a result, the total magnetization is given by a 91:9 small:large weighting of the individual magnetizations (see Table I). The Brownian rotation

times differ by a factor of 10. The BD simulation results are compared to the Weiss theory, and the expressions for noninteracting particles [Eq. (16)]. First, the Weiss theory and BD simulations are in qualitative agreement, with the initial decays corresponding to Eq. (16), and the asymptotic decays corresponding to longer relaxation times (to be discussed in Sec. III E). For each fraction, the results for noninteracting particles are monotonic, and only agree with the Weiss theory and BD simulations at short times, illustrating the large effects of dipole-dipole interactions. Secondly, although the Weiss theory is qualitatively correct, the agreement with BD simulations is not perfect, except for the small particles; the effective relaxation times are larger in the simulations than from the theory. Table I shows that the individual dipolar coupling constants for the small and large particles are $\lambda = 0.55$ and 5.5, respectively. With $\lambda \gtrsim 4$, chainlike correlations are anticipated [37], which will not be captured by the theory. Therefore, the Weiss theory and BD simulations differ in the cases of the large-particle and total relaxation curves. The agreement is generally much better for the small particles, but there are still deviations because of the effects of the large particles on the small ones. Finally, the prediction from the Weiss theory is that, at long times, each fraction in the sample relaxes with the same effective time. To some extent, this is borne out by the BD simulations, but the small-fraction curve is too noisy to be sure. The effective relaxation times are discussed further in Sec. III E.

B. Bidisperse configuration B

Magnetic relaxation curves for bidisperse configuration B are shown in Fig. 2. The small and large particles make equal contributions to the saturation magnetization of the ferrofluid, but the Brownian rotation times differ by a factor of 10. Overall, the agreement between Weiss theory and BD simulations is much better than that for configuration A. This is
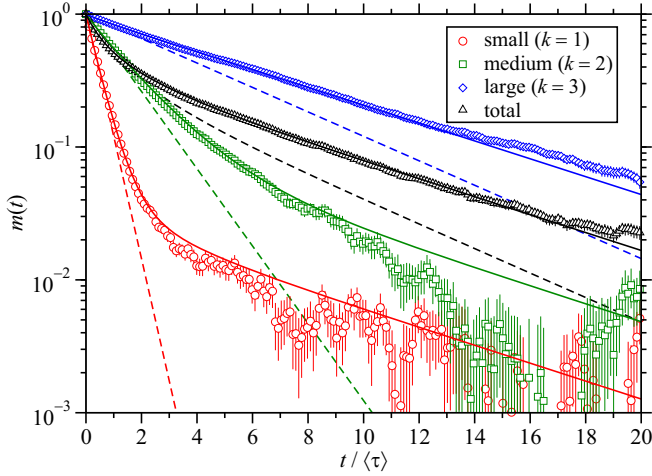
FIG. 3. Magnetic relaxation curves for tridisperse configuration C. The points are from BD simulations, the dashed lines are for non-interacting particles, and the solid lines are from the Weiss theory: red circles and lines, small particles ($k = 1$); green squares and lines, medium particles ($k = 2$); blue diamonds and lines, large particles ($k = 3$); black triangles and lines, all particles.

FIG. 4. Magnetic relaxation curves for bidisperse configuration D. The points are from BD simulations, the dashed lines are for noninteracting particles, and the solid lines are from the Weiss theory: red circles and lines, small particles ($k = 1$); blue diamonds and lines, large particles ($k = 2$); black triangles and lines, all particles.

because the dipolar coupling constant for each fraction is not too large, and therefore the theory is expected to be accurate. The results for noninteracting particles are inaccurate, except at short times, highlighting the importance of dipole-dipole interactions. The results show that interactions lead to a clear increase in the relaxation time of the small particles. As with configuration A, the Weiss theory predicts that the asymptotic relaxation times are the same for each fraction, but in this case, the simulation results confirm it, at least superficially. A comparison between theory and simulation should be possible, and Fig. 2 shows exponential fits to the asymptotic portions of the relaxation curves from BD simulations. The corresponding relaxation times will be compared to theoretical predictions in Sec. III E.

C. Tridisperse configuration C

An interesting extension is to study a system with more than two fractions. Magnetic relaxation curves for tridisperse configuration C are shown in Fig. 3. The small, medium, and large particles make equal contributions to the saturation magnetization, and the Brownian rotation times span an order of magnitude. For each fraction, there is an apparent crossover from short-time, rapid relaxation, to long-time, slow relaxation. As before, the Weiss theory predicts the same asymptotic decay time for each fraction. The BD simulation results for the small and medium particles are noisy, despite averaging over 50 independent simulations, but they are at least consistent with the predictions from the Weiss theory. The results for noninteracting particles are only correct at short times.

D. Bidisperse configuration D

Magnetic relaxation curves for bidisperse configuration D are shown in Fig. 4. Here the small-particle fraction is fixed at $p_1 = 0.9$, and the Brownian rotation times differ by only
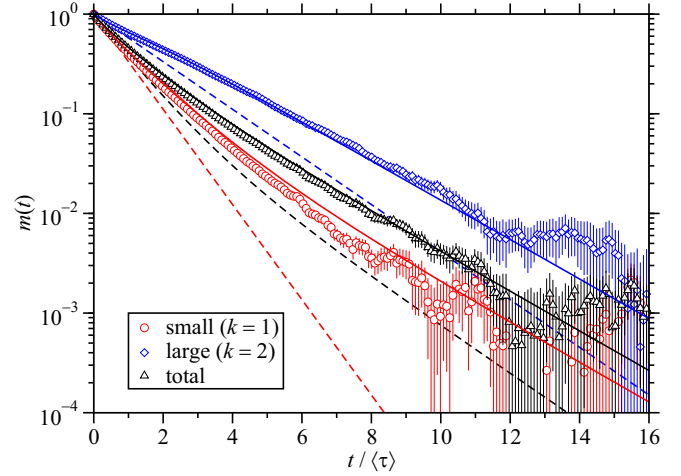
a factor of 2. As will be shown in Sec. III E, this system is predicted to show some interesting behavior in the effective relaxation times. Despite the statistical scatter in the BD simulation data, the agreement with Weiss theory is adequate. Since the Brownian rotation times of the two fractions are not very dissimilar, there is not such a clear crossover from the short-time to long-time regimes, but the variations with time are discussed in more detail in Sec. III E. The error bars for the small-particle and large-particle fractions at long times are comparable, because the magnetizations are more similar than in the other configurations.

E. Effective relaxation times

The general appearance of the magnetic relaxation curves for configurations A–D have been surveyed, and the effective relaxation times are presented next. Figure 5 shows the predictions for $\tau_{\rm eff}$ [Eq. (17)] from the Weiss theory. Results are shown for each configuration, each particle type, and for the overall magnetization. Figure 5(a) shows the results for configuration A. As shown in Sec. II B, the initial decay of the magnetization is dictated by the Brownian rotation time for each fraction. Combining Eqs. (16), (17), and (21), the initial ($t = 0$) relaxation time for the total magnetization is

$$\tau_{\rm eff} = \frac{\langle \mu \rangle}{\langle \mu \tau^{-1} \rangle}, \tag{22}$$

and because both μ and τ are proportional to σ^3, $\tau_{\rm eff} = \langle \tau \rangle$. So, as per Eq. (16), the initial decay times are as for noninteracting particles, but with increasing time, the small-particle effective relaxation time increases, and converges with that of the large particles. In addition, the effective relaxation time of the large particles shows a local maximum, then a local minimum, and then an asymptotic value larger than the Brownian rotation time. The local maximum occurs because with increasing time, the interactions with all other particles lead to an initial increase in the relaxation time, while the decaying
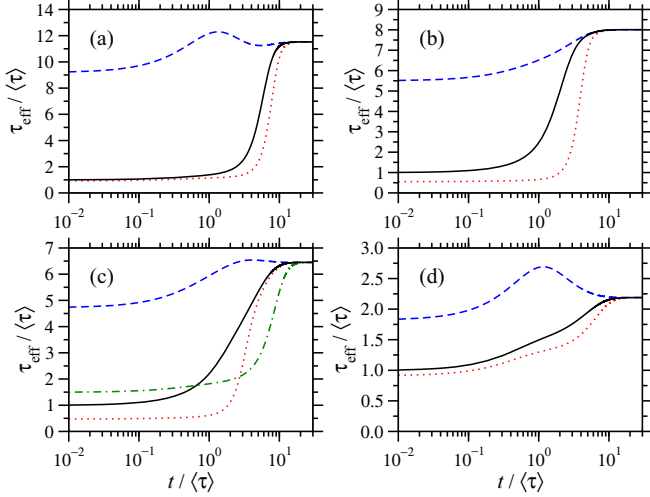
FIG. 5. Effective relaxation times from the Weiss theory for (a) bidisperse configuration A, (b) bidisperse configuration B, (c) tridisperse configuration C, and (d) bidisperse configuration D: red dotted lines, small particles; green dot-dashed lines, medium particles; blue dashed lines, large particles; black solid lines, all particles.

magnetization of the small particles leads to a subsequent decrease in the relaxation time.

The asymptotic relaxation time can be determined by rewriting Eq. (15) for the small particles as

$$\frac{dm_1}{dt} = -\frac{m_1}{\tau_1}\left[1 - \frac{\chi_1}{3} - \frac{\chi_2}{3}\left(\frac{\mu_1 m_2}{\mu_2 m_1}\right)\right], \qquad (23)$$

from which the effective relaxation time is

$$\tau_{\text{eff},1} = \frac{3\tau_1}{3 - \chi_1 - \chi_2(\mu_1 m_2/\mu_2 m_1)}. \qquad (24)$$

A similar equation can be written for $\tau_{\text{eff},2}$ by exchanging the labels. The fact that the two effective relaxation times approach a common, constant value means that the ratio m_1/m_2 also becomes constant (call it C_{12}). Therefore

$$\frac{3\tau_1}{3 - \chi_1 - \chi_2(\mu_1/\mu_2)C_{12}^{-1}} = \frac{3\tau_2}{3 - \chi_2 - \chi_1(\mu_2/\mu_1)C_{12}}, \qquad (25)$$

and so C_{12} is given by

$$C_{12} = \frac{m_1}{m_2} = \frac{-b + \sqrt{b^2 - 4ac}}{2a} \qquad (26)$$

with

$$a = \tau_1\chi_1\left(\frac{\mu_2}{\mu_1}\right), \qquad (27a)$$

$$b = 3(\tau_2 - \tau_1) + \tau_1\chi_2 - \tau_2\chi_1, \qquad (27b)$$

$$c = -\tau_2\chi_2\left(\frac{\mu_1}{\mu_2}\right). \qquad (27c)$$

Putting in the values from Table I gives $C_{12} \simeq 0.02211$ and $\tau_{\text{eff}} \simeq 11.53\langle\tau\rangle$ for both fractions, and hence the total as well.

Figure 5(b) shows the same kind of results for configuration B. The basic picture is similar to that for configuration A,

except that the large-particle effective relaxation time does not show any inflections; it increases from the initial, Brownian value to a larger value. The common asymptotic value for all fractions can be computed by the same approach outlined above, which gives $C_{12} \simeq 0.03363$ and $\tau_{\text{eff}} \simeq 8.008\langle\tau\rangle$. In this case, the BD simulation data are just about adequate for getting an estimate of the asymptotic times. As shown in Fig. 2, it is possible to fit the magnetization curves over the range $5 \leqslant t/\langle\tau\rangle \leqslant 30$ with the function $\ln m(t) = A - t/\tau_{\text{eff}}$. This gives $\tau_{\text{eff},1} = 8.94(20)\langle\tau\rangle$ for the small particles, $\tau_{\text{eff},2} = 8.549(11)\langle\tau\rangle$ for the large particles, and $\tau_{\text{eff}} = 8.514(12)\langle\tau\rangle$ for the total. These values are slightly larger than the asymptotic relaxation time from the Weiss theory, but the small deviations can be explained by the theory not capturing the interactions fully.

Figure 5(c) shows the effective relaxation times for the three fractions in configuration C, and the total. The large-particle relaxation time shows a small maximum before approaching its asymptotic value, while the relaxation times for the small and medium particles increase in a less complex way. There are now two asymptotic magnetization ratios, being $C_{12} = m_1/m_2 \simeq 0.2622$ and $C_{23} = m_2/m_3 \simeq 0.1103$. The effective relaxation time approaches $\tau_{\text{eff}} \simeq 6.450\langle\tau\rangle$.

Figure 5(d) shows the results for configuration D, the parameters of which were chosen because of the unusual behavior of the effective relaxation times. In this case, the large-particle relaxation time shows a local maximum, as seen in configurations A and C, but now the small-particle relaxation time shows a point of inflection at around the same value of t. The existence of a point of inflection is interesting, and it can be understood as follows. Because the configuration is almost monodisperse, the short-time relaxation of the small particles is affected mainly by the small-particle magnetization; the absolute large-particle magnetization is much smaller, and relaxes more slowly. Hence, the small particles show the normal crossover from the Brownian relaxation time, to an effective relaxation time given approximately by Eq. (18) and $\tau_{\text{eff},1} = \tau_1/(1 - \chi_1/3) \simeq 1.182$. Eventually, the small-particle magnetization becomes smaller than the large-particle magnetization, the ratio approaches $C_{12} \simeq 0.1449$, and the asymptotic relaxation time is $\tau_{\text{eff}} \simeq 2.189\langle\tau\rangle$.

The width of the first plateau can be enhanced by increasing the proportion of small particles; this is the reason for defining configuration E in Table I. Theoretical results for configuration E are shown in Fig. 6. The first plateau is close to $\tau_{\text{eff},1} = \tau_1/(1 - \chi_1/3) \simeq 1.457\langle\tau\rangle$, the asymptotic magnetization ratio is $C_{12} \simeq 0.03292$, and the corresponding effective relaxation time is $\tau_{\text{eff}} \simeq 2.050\langle\tau\rangle$.

One of the most interesting predictions from the theory is that all fractions have the same asymptotic effective relaxation time. For the most part, it is difficult to test this directly with the BD simulation data because of the statistical scatter, and the problem of reliable numerical differentiation. Note that the relevant portions of the relaxation curves are where $m_k(t) \lesssim 0.01$; thermal fluctuations around $m_k = 0$ are unavoidable, and in fact linear response theory relates these to the dynamic magnetic susceptibility. But the theoretical prediction can be tested qualitatively by plotting some simple ratios. At long times, if the magnetization is assumed to decay like $m_k(t) \approx \exp(-t/\tau_{\text{eff},k})$, and if two different fractions k
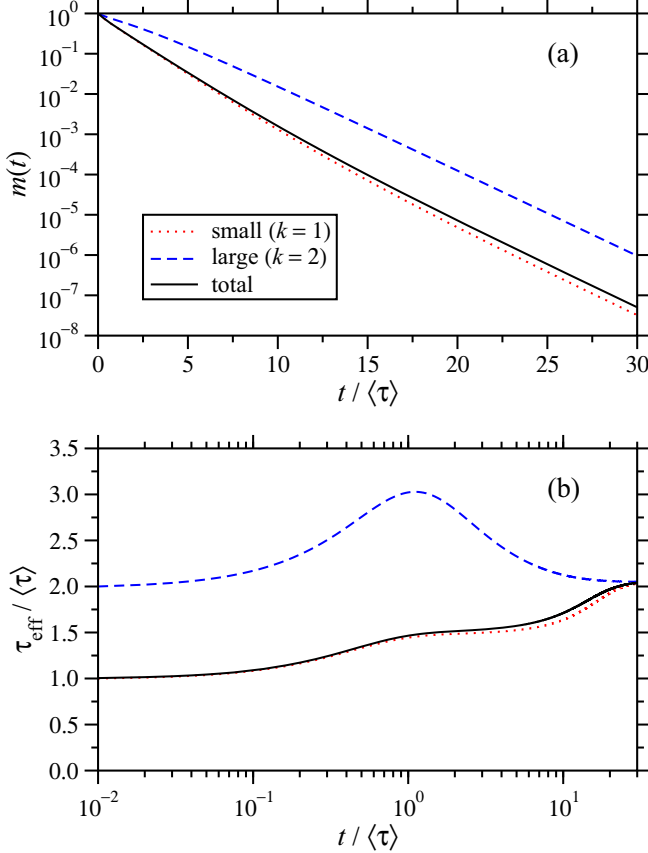
FIG. 6. Magnetic relaxation curves (a) and effective relaxation times (b) from the Weiss theory for configuration E: red dotted lines, small particles ($k = 1$); blue dashed lines, large particles ($k = 2$); black solid lines, all particles.

and l decay at the same rate, then

$$\frac{m_k(t)}{m_l(t)} \approx \text{const.} \tag{28}$$

Note that, in the noninteracting case, the ratio for two different fractions decays monotonically with a relaxation time $\tau_k \tau_l / (\tau_l - \tau_k)$. With interactions, the Weiss theory predicts that $m_1 / m_2 = C_{12}$ and $m_2 / m_3 = C_{23}$ approach constant values. In all cases, the ratio of the total magnetization and the magnetization for the slowest-relaxing (largest) particles tends to a constant because at long times, the magnetization of the other fractions will have decayed much more, and so

$$\frac{m(t)}{m_{\text{large}}(t)} = \frac{\sum_k p_k \mu_k m_k(t)}{\langle \mu \rangle m_{\text{large}}(t)} \simeq \frac{p_{\text{large}} \mu_{\text{large}}}{\langle \mu \rangle}. \tag{29}$$

Any residual magnetization from the smaller fractions will give a slightly larger number. Figure 7 shows plots of such ratios for configurations A–D; because the fraction of large particles in configuration E is so small, BD simulations are impractical. Note that in all cases, the results for noninteracting particles are as explained above: the small/large ratio decays monotonically, and the total/large ratio tends to a known constant. For configuration A, the small/large and total/large magnetization ratios do indeed appear to level off at long
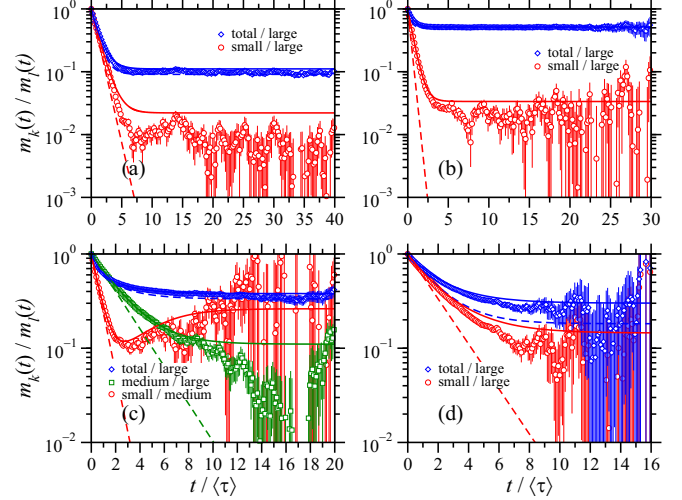
FIG. 7. Ratios of the magnetization of different fractions in (a) bidisperse configuration A, (b) bidisperse configuration B, (c) tridisperse configuration C, and (d) bidisperse configuration D. The points are from BD simulations, the dashed lines are for noninteracting particles, and the solid lines are from the Weiss theory. The small/large and small/medium ratios are shown as red circles and red lines, the medium/large ratio in (c) is shown as green squares and green lines, and the total/large ratios are shown as blue diamonds and blue lines. For each configuration, the theoretical and simulation results for the total/large ratio are in good agreement within the estimated errors, and so the points and lines overlap.

times. The agreement between theory and simulation is moderate, as per the magnetic relaxation curves themselves. For configuration B, the agreement between theory and simulation is better, and again, the simulation results confirm that the small/large and total/large magnetization ratios tend towards constants. For configuration C, the behavior is more complex. The total/large magnetization ratio tends toward a constant value, and the agreement between theory and simulation is good. The small/medium magnetization ratio first decreases, and then increases before reaching a plateau. The simulation results capture the predicted local minimum accurately, and although there is a lot of scatter at long times, and the error bars are large, the results are not inconsistent with theory. The main source of scatter is the magnetization of the medium particles at long times, but the initial decrease before $t \simeq 10 \langle \tau \rangle$ is in agreement with theory. For configuration D, the agreement between theory and simulation is reasonably good, and the simulation results appear to be leveling off. Because the small and large particles have similar Brownian rotation times, the respective magnetizations are not very different at long times, and so the error bars are large for both ratios being presented. In summary, although the BD simulation data are noisy at long times, the results for configurations A and B clearly support the theoretical prediction that the effective relaxation times for all particle fractions are asymptotically equal, and quite different from the individual Brownian rotation times for noninteracting particles. For configurations C and D the simulation results agree with theory at short times, and are not inconsistent with the predictions at long times, despite substantial error bars.

IV. CONCLUSIONS

The magnetic relaxation dynamics in polydisperse ferrofluids have been studied using theory and Brownian-dynamics simulations. The theory is based on the Fokker-Planck-Brown equation for the Brownian rotation of spherical particles. The effects of magnetic dipole-dipole interactions on the relaxation dynamics were included using a Weiss-theory approach. The resulting equations were solved numerically to give the magnetic relaxation curve for each fraction in the ferrofluid, as well as the total magnetization. The main predictions of the theory are that the relaxation times increase significantly as a result of the interactions, and that at long times, every fraction in the ferrofluid has the same relaxation time, which is longer than any of the individual Brownian rotation times. An analytical expression for the asymptotic relaxation time was obtained. The theory was compared to Brownian dynamics simulations of several types of bidisperse and tridisperse ferrofluids. In general, the simulation results support the theoretical predictions, although a direct comparison of the asymptotic effective relaxation times was difficult because of the statistical scatter in the numerical data. But by comparing magnetization ratios for individual fractions, which should tend towards constant values if the relaxation times are the same, it is clear that the basic picture is confirmed. This work provides some useful new information on what to expect from magnetic relaxation experiments on real ferrofluids in which particle-size polydispersity is practically unavoidable. The main message is that interactions and polydispersity have significant effects on the magnetic relaxation dynamics, and that these must be taken into account if experimental measurements are to be used to infer anything about the constituent magnetic particles, or the structures that they form. The extension of the theory to ferrofluids with continuous particle-size distributions is straightforward, and done most easily by splitting up the distribution into a large number of discrete fractions. The distinction between small and large particles then becomes blurred, but having tested the theory in detail for bidisperse and tridisperse systems, this extension can be done with confidence as long as the interactions are not too strong. If the magnetic dipole-dipole interactions between some or all fractions are strong, then the particles will form chainlike clusters in an aligning field, and this introduces three significant complications: first, there will be polydispersity in terms of cluster size and composition [27]; second, the clusters will evolve during the magnetic relaxation process; and third, the intrinsic dynamics of clusters are complicated [38]. All of these present considerable theoretical challenges, but it may be possible to incorporate effective relaxation times for clusters, and estimates of the (equilibrium) cluster-size distributions, into the current theory.

[1] R. E. Rosensweig, *Ferrohydrodynamics* (Dover Publications, New York, 1998).

[2] R. E. Rosensweig, Heating magnetic fluid with alternating magnetic field, J. Magn. Magn. Mater. **252**, 370 (2002).

[3] Q. A. Pankhurst, J. Connolly, S. K. Jones, and J. Dobson, Applications of magnetic nanoparticles in biomedicine, J. Phys. D: Appl. Phys. **36**, R167 (2003).

[4] Q. A. Pankhurst, N. T. K. Thanh, S. K. Jones, and J. Dobson, Progress in applications of magnetic nanoparticles in biomedicine, J. Phys. D: Appl. Phys. **42**, 224001 (2009).

[5] A. F. Pshenichnikov, V. V. Mekhonoshin, and A. V. Lebedev, Magneto-granulometric analysis of concentrated ferrocolloids, J. Magn. Magn. Mater. **161**, 94 (1996).

[6] A. O. Ivanov, S. S. Kantorovich, E. N. Reznikov, C. Holm, A. F. Pshenichnikov, A. V. Lebedev, A. Chremos, and P. J. Camp, Magnetic properties of polydisperse ferrofluids: A critical comparison between experiment, theory, and computer simulation, Phys. Rev. E **75**, 061405 (2007).

[7] S. A. Sokolsky, A. Yu. Solovyova, V. S. Zverev, M. Hess, A. Schmidt, and E. A. Elfimova, Analysis of the ferrofluid microstructure based on the static magnetic measurements, J. Magn. Magn. Mater. **537**, 168169 (2021).

[8] A. O. Ivanov, O. B. Kuznetsova, and P. J. Camp, Dynamic magnetogranulometry of ferrofluids, J. Magn. Magn. Mater. **498**, 166153 (2020).

[9] A. S. Ivanov, A. Yu. Solovyova, V. S. Zverev, and E. A. Elfimova, Distribution functions of magnetic moments and relaxation times for magnetic fluids exhibiting controllable microstructure evolution, J. Mol. Liq. **367**, 120550 (2022).

[10] M. Küster, F. Ludwig, A. Eremin, P. H. Boštjančič, D. Lisjak, N. Sebastián, A. Mertelj, and H. Nádasi, Magnetic dynamics in suspensions of ferrimagnetic platelets, J. Mol. Liq. **360**, 119484 (2022).

[11] D. Eberbeck, S. Hartwig, U. Steinhoff, and L. Trahms, Description of the magnetisation decay in ferrofluids with a narrow particle size distribution, Magnetohydrodynamics **39**, 77 (2003).

[12] F. Ludwig, S. Mäuselein, E. Heim, and M. Schilling, Magnetorelaxometry of magnetic nanoparticles in magnetically unshielded environment utilizing a differential fluxgate arrangement, Rev. Sci. Instrum. **76**, 106102 (2005).

[13] D. Eberbeck, F. Wiekhorst, U. Steinhoff, and L. Trahms, Aggregation behaviour of magnetic nanoparticle suspensions investigated by magnetorelaxometry, J. Phys.: Condens. Matter **18**, S2829 (2006).

[14] F. Ludwig, E. Heim, D. Menzel, and M. Schilling, Investigation of superparamagnetic Fe_3O_4 nanoparticles by fluxgate magnetorelaxometry for use in magnetic relaxation immunoassays, J. Appl. Phys. **99**, 08P106 (2006).

[15] F. Ludwig, E. Heim, and M. Schilling, Characterization of superparamagnetic nanoparticles by analyzing the magnetization and relaxation dynamics using fluxgate magnetometers, J. Appl. Phys. **101**, 113909 (2007).

[16] F. Wiekhorst, U. Steinhoff, D. Eberbeck, and L. Trahms, Magnetorelaxometry assisting biomedical applications of magnetic nanoparticles, Pharm. Res. **29**, 1189 (2012).

[17] J. Dieckhoff, D. Eberbeck, M. Schilling, and F. Ludwig, Magnetic-field dependence of Brownian and Néel relaxation times, J. Appl. Phys. **119**, 043903 (2016).

[18] J. Fock, C. Balceris, R. Costo, L. Zeng, F. Ludwig, and M. F. Hansen, Field-dependent dynamic responses from dilute magnetic nanoparticle dispersions, Nanoscale **10**, 2052 (2018).

[19] P. Lemal, S. Balog, L. Ackermann-Hirschi, P. Taladriz-Blanco, A. M. Hirt, B. Rothen-Rutishauser, M. Lattuada, and A. Petri-Fink, Simple and fast evaluation of relaxation parameters of magnetic nanoparticles, J. Magn. Magn. Mater. **499**, 166176 (2020).

[20] A. O. Ivanov and P. J. Camp, Effects of interactions, structure formation, and polydispersity on the dynamic magnetic susceptibility and magnetic relaxation of ferrofluids, J. Mol. Liq. **356**, 119034 (2022).

[21] J. O. Sindt, P. J. Camp, S. S. Kantorovich, E. A. Elfimova, and A. O. Ivanov, Influence of dipolar interactions on the magnetic susceptibility spectra of ferrofluids, Phys. Rev. E **93**, 063117 (2016).

[22] A. O. Ivanov and P. J. Camp, Effects of interactions on magnetization relaxation dynamics in ferrofluids, Phys. Rev. E **102**, 032610 (2020).

[23] A. O. Ivanov and P. J. Camp, Theory of the dynamic magnetic susceptibility of ferrofluids, Phys. Rev. E **98**, 050602(R) (2018).

[24] W. F. Brown, Jr., Thermal fluctuations of a single-domain particle, J. Appl. Phys. **34**, 1319 (1963).

[25] W. F. Brown, Jr., Thermal fluctuations of a single-domain particle, Phys. Rev. **130**, 1677 (1963).

[26] W. F. Brown, Jr., Thermal fluctuation of fine ferromagnetic particles, IEEE Trans. Magn. **15**, 1196 (1979).

[27] A. O. Ivanov and S. S. Kantorovich, Chain aggregate structure and magnetic birefringence in polydisperse ferrofluids, Phys. Rev. E **70**, 021401 (2004).

[28] E. Novak, E. Minina, E. Pyanzina, S. Kantorovich, and A. Ivanov, Structure factor of model bidisperse ferrofluids with relatively weak interparticle interactions, J. Chem. Phys. **139**, 224905 (2013).

[29] Yu. E. Nekhoroshkova, O. A. Goldina, P. J. Camp, E. A. Elfimova, and A. O. Ivanov, Partial correlations in a bidisperse ferrofluid in an external magnetic field: Theory and computer simulations, J. Exp. Theor. Phys. **118**, 442 (2014).

[30] B. F. Edwards, D. M. Riffe, J.-Y. Ji, and W. A. Booth, Interactions between uniformly magnetized spheres, Am. J. Phys. **85**, 130 (2017).

[31] A. O. Ivanov, V. S. Zverev, and S. S. Kantorovich, Revealing the signature of dipolar interactions in dynamic spectra of polydisperse magnetic nanoparticles, Soft Matter **12**, 3507 (2016).

[32] P. Weiss, L'hypothèse du champ moléculaire et la propriété ferromagnétique, J. Phys. Theor. Appl. **6**, 661 (1907).

[33] *Mathcad 14.0 (Academic Version)* (PTC, Boston, 2007).

[34] LAMMPS Molecular Dynamics Simulator, https://www.lammps.org (2023).

[35] S. Plimpton, Fast parallel algorithms for short-range molecular dynamics, J. Comput. Phys. **117**, 1 (1995).

[36] A. P. Thompson, H. M. Aktulga, R. Berger, D. S. Bolintineanu, W. M. Brown, P. S. Crozier, P. J. in't Veld, A. Kohlmeyer, S. G. Moore, T. D. Nguyen *et al.*, LAMMPS—A flexible simulation tool for particle-based materials modeling at the atomic, meso, and continuum scales, Comput. Phys. Commun. **271**, 108171 (2022).

[37] J. J. Weis and D. Levesque, Chain Formation in Low Density Dipolar Hard Spheres: A Monte Carlo Study, Phys. Rev. Lett. **71**, 2729 (1993).

[38] P. J. Camp, A. O. Ivanov, and J. O. Sindt, How chains and rings affect the dynamic magnetic susceptibility of a highly clustered ferrofluid, Phys. Rev. E **103**, 062611 (2021).